Preparation of Gas Phase Naked Silver Cluster Cations Outside the Mass Spectrometer from Ligand Protected Clusters in Solution

SCHOLARONE™
Manuscripts

Preparation of Gas Phase Naked Silver Cluster Cations Outside the Mass Spectrometer from Ligand Protected Clusters in Solution

Madhuri Jash,[a] Arthur C. Reber,[b] Atanu Ghosh,[a] Depanjan Sarkar,[a] Md Bodiuzzaman,[a] Pallab Basuri,[a] Ananya Baksi,[a] Shiv N. Khanna,[b] and Thalappil Pradeep*[a]*

[a]DST Unit of Nanoscience (DST UNS) and Thematic Unit of Excellence (TUE), Department of Chemistry, Indian Institute of Technology Madras, Chennai 600 036, India

[b]Department of Physics, Virginia Commonwealth University, Richmond, Virginia 23284, United States

AUTHOR INFORMATION

Corresponding Authors

* Email: pradeep@iitm.ac.in

* Email: snkhanna@vcu.edu

ABSTRACT

Gas phase clusters of noble metals, prepared by laser desorption from the bulk have been investigated extensively in vacuum using mass spectrometry. However, such clusters have not been known to exist in ambient conditions till date. In our previous work, we have shown that in-

source fragmentation of ligands can be achieved starting from hydride and phosphine co-protected silver clusters leading to naked silver clusters inside the mass spectrometer. In a recent series of experiments, we have found that systematic desorption of ligands of the monolayer protected atomically precise silver cluster can also occur in the atmospheric gas phase. Here, we present the results, wherein, $[Ag_{18}H_{16}(TPP)_{10}]^{2+}$ (TPP = triphenylphosphine) cluster results in the formation of naked cluster, Ag_{17}^{+} along with $Ag_{18}H^{+}$ without mass selection, outside the mass spectrometer, in air. These cationic naked metal clusters are made by passing electrosprayed ligand protected clusters through a heated tube, in the gas phase. Reactions with oxygen suggest Ag_{17}^{+} to be more reactive than $Ag_{18}H^{+}$, in agreement with their electronic structures. The more common thiolate protected clusters produce fragments of metal thiolates under identical processing conditions and no naked clusters were observed.

KEYWORDS naked clusters, atomically precise clusters, mass spectrometry gas phase reactions, oxygen, HOMO-LUMO gap.

INTRODUCTION

Atomically precise clusters of noble metals composed of a metal core and a ligand shell, with precise composition, structure and properties also referred to as aspicules, constitute one of the most expanding areas of nanomaterials science in the recent past.[1-7] For monolayer protected clusters, to observe substantial catalytic activity, complete removal of the protecting ligands is essential which has been difficult for solution phase synthesized clusters. In 1986, Schmid and Klein first reported the formation of ligand free M_{13} (M = Au, Rh, Ru) clusters from ligand stabilized M_{55} clusters by electrophoresis.[8] The catalytic properties of such clusters due to electronic confinement as well as unique geometry have been explored in the supported form.[9-13] Getting ligand free metal cores on solid supports by using high temperature often results in broad particle size distributions with loss of atomicity.[14] On the other hand, these solution phase ligand protected clusters have shown their systematic fragmentation in vacuum, often leading to metal ligand fragments in mass spectrometric studies.[15-17] While sequential loss of ligands, producing small metal clusters is likely, no intact cluster core has been observed so far in ambient air.

From early 1970s, the production and reaction of free gas phase clusters have been demonstrated by using various cluster sources, using laser vaporization, ion traps, flow-tube reactors and improved mass spectrometers. Detailed information on the structural and electronic properties of gas phase naked clusters (NCs) validate their distinct character, much different from ligand protected metal clusters in the free and supported forms.[18, 19] The reactivity of NCs not only depend on their charge, size and intrinsic activity but also to the chemisorption, bond cleavage energy and polarity of the reacted molecules.[18,20] But to obtain specific catalytic activity

of a gas phase cluster, with particular atomicity, mass selection is needed to obtain satisfactory precision.

Although smaller naked metal clusters have been made by various processes such as thermal desorption, sputtering, laser desorption and electrospray ionization, starting from bulk metals or salts, no monolayer protected cluster was used for such investigations before. Recently, Whetten and Brodbelt have shown that by using deep UV irradiation at 193 nm (6.4 eV), NCs like Au_4^+ to Au_{20}^+ can be formed along with their ligand-containing product ions within the mass spectrometer in vacuum starting from ligand protected gold clusters, $Au_{25}(SR)_{18}$ and $Au_{36}(SR)_{24}$.[21] The inherent instability of the intact cluster core and the stability of the metal thiolate complexes make the observation of the intact cluster core difficult.[22-24] Extensive mass spectrometric studies have been done on ligated (mainly diphosphine) silver hydride nanoclusters by O'Hair group, which show that all hydrides can be removed as H_2 but complete removal of other ligands is not possible even using a laser.[25, 26] Also, there have been extensive studies on synthesis and reactivity of copper, silver and gold hydride complexes.[27] The recent identification of hydride and phosphine co-protected clusters of silver[28] and the weak ligand-metal interaction in such systems made us explore the formation of silver NCs within the mass spectrometer by in-source fragmentation and the results of these studies have been reported recently.[29] In our current experiment, we have observed that thermal activation of the electrosprayed cluster, $[Ag_{18}H_{16}(TPP)_{10}]^{2+}$ produced highly monodispersed NC ions, Ag_{17}^+ and $Ag_{18}H^+$ in atmospheric gas phase. The ability to create such atomically precise pieces of metals outside the mass spectrometer will allow exploration of their unknown chemistry, glimpses of such studies are also presented here. We note that the method of atmospheric pressure thermal dissociation was first introduced to make peptide and protein ions.[30, 31] Then the method was

extended to silver salts where extremely small clusters such as Ag_3^+ and Ag_7^- were produced during mass spectrometric analysis, by varying the source parameters.[32] Such methods have never been applied to monolayer protected atomically precise metal clusters.

Compared to the bulk and monolayer protected silver clusters, NCs can have very different chemical reactivity due to their unique electronic and geometric structures.[33, 34] Density functional theory (DFT) calculations have shown that the dissociation of molecular oxygen was favored in larger sized silver NCs.[35] Electronic states in metallic clusters including silver clusters can be rationalized using the model of confined nearly free electron gas. For compact clusters, such a description leads to the grouping of states into shells that can be labelled as 1S, 1P, 1D, 2S, etc., much the same way as in atoms.[36] The numbers and upper case letters indicate the principal and angular momentum quantum numbers of the delocalized orbitals. The ground state of oxygen is a spin triplet and any activation of the oxygen molecule requires a virtual spin excitation of the cluster to accommodate the spin.[37, 38] For clusters with singlet ground states such a spin accommodation requires a spin excitation from the singlet to the triplet configuration whose energy is determined by the gap between the highest occupied molecular orbital (HOMO) and the lowest unoccupied molecular orbital (LUMO). Consequently, clusters with high HOMO-LUMO gap are resistant to reactions with oxygen. Here we show that the dissociation of molecular oxygen and its attachment with Ag_{17}^+ happen due to the preferred HOMO-LUMO gap in the metal core. In contrast, $Ag_{18}H^+$ shows resistance to reaction with oxygen due to the cluster's comparatively high HOMO-LUMO gap.

EXPERIMENTAL SECTION

Reagents and Materials. Silver nitrate ($AgNO_3$, 99.9%) was purchased from Rankem India, triphenylphosphine (TPP, 99%), sodium borohydride ($NaBH_4$, 98%), sodium borodeuteride

(NaBD$_4$, 98 atom% D) and methanol-d$_4$ (CD$_3$OD, 99.8 atom% D) were purchased from Sigma-Aldrich and used without further purification. HPLC grade methanol (MeOH) was from Finar chemicals and analytical grade chloroform (CHCl$_3$) was from Rankem India. All the chemicals were used without further purification unless otherwise mentioned. Millipore water, obtained from Milli-Q (Millipore apparatus) with a resistivity of 18.2 MΩ.cm was used for all the experiments.

Synthesis. The cluster [Ag$_{18}$H$_{16}$(TPP)$_{10}$]$^{2+}$ was synthesized by using a small modification of the reported method by Bootharaju et al.[28] In the first step, the silver precursor (20 mg of AgNO$_3$) was taken in 5 mL of MeOH in a 100 ml round bottom flask and 70 mg of triphenylphosphine solution in 10 mL of chloroform was added under stirring at room temperature. After 20 minutes of reaction, 6 mg of NaBH$_4$ in 0.5 mL of ice cold Millipore water was added. After addition of NaBH$_4$ the color changed immediately from colorless to light yellow. To avoid any further oxidation of silver, the entire synthesis procedure was carried out under dark condition. Over three hours of continuous stirring in dark condition, the light yellow reaction mixture became dark green which indicated the formation of [Ag$_{18}$H$_{16}$(TPP)$_{10}$]$^{2+}$ cluster. The solution was vacuum evaporated at room temperature and then to remove the excess silver precursor and NaBH$_4$, 20-22 mL cold Millipore water was added to the residue and the mixture was sonicated for 2 minutes. After sonication, the solution was centrifuged at 3,000 rpm for 5 minutes and a residue was separated. The supernatant containing soluble impurities was discarded and the precipitate consisting of [Ag$_{18}$H$_{16}$(TPP)$_{10}$]$^{2+}$ cluster was dissolved in 10 mL methanol and the solution was rotavaporated at room temperature to make a dry sample. The solid green sample was collected and dissolved in 2 mL methanol and centrifuged for 5 minutes at 5,000 rpm to remove excess TPP ligands. The deep green [Ag$_{18}$H$_{16}$(TPP)$_{10}$]$^{2+}$ cluster solution

was used for further characterization. For mass spectrometry experiments, 100 µL of the green

solution was diluted to 1 mL by methanol. For synthesizing the deuterated Ag_{18} analogue, a

similar method was followed by replacing the $NaBH_4$ with $NaBD_4$.

Instrumentation. UV-vis spectra of nanoclusters were recorded using a Perkin Elmer

Lambda 25 UV-Vis spectrometer. Absorption spectra were typically measured in the range of

200-1100 nm with a band pass filter of 1 nm. The high resolution mass spectra of

$[Ag_{18}H_{16}(TPP)_{10}]^{2+}$ and $[Ag_{18}D_{16}(TPP)_{10}]^{2+}$ were recorded using a Waters Synapt G2Si High

Definition Mass Spectrometer (abbreviated as G2Si subsequently) equipped with electrospray

ionization (ESI) source. This mass spectrometer is a combination of electrospray source,

quadrupole ion guide/trap, ion mobility cell and TOF analyzer. These cluster samples were

prepared in methanol and were infused into the instrument at a flow rate of 30 µL/min. The

capillary voltage was kept at 2 kV and to avoid any in-source fragmentation, both the cone

voltage and source offset were kept at 0 V. All other experiments, including the characterization

of NCs described in this paper were carried out by using Thermo Scientific LTQ XL Linear Ion

Trap Mass Spectrometer (abbreviated as LTQ subsequently) with a home-built nano-ESI source.

Photograph of the instrumental set-up is shown in supporting information S1. The LTQ mass

spectrometer is a combination of electrospray source, ion sweep cone, ion transfer capillary,

quadrupole, octapole and two-dimensional linear ion trap. The following instrumental parameters

were used for all over the experiments to get a good ion signal without fragmentation. Solvent:

methanol; flow rate: 3 µL/min; ionization spray voltage: 3 kV; capillary voltage (abbreviated as

CV): 45 V and tube lens voltage (abbreviated as TV): 100 V. All the mass spectrometric

measurements were done in the positive ion mode. Tandem mass spectrometric (MS/MS or MS^2)

measurements were done by using ultra high-pure helium gas (99.995%) in the LTQ mass

spectrometer. In the MS/MS studies, mass selected ions were fragmented in the ion trap by colliding with helium. During the CID or MS^2 experiments, the injection time was 300 ms and 5 microscans were averaged with an activation time (time for which the resonance excitation RF voltage was applied) of 30 ms. An activation Q value of 0.25 was applied and the isolation width and collision energy were optimized according to the particular precursor ion. Transmission electron microscopy (TEM) and high-resolution transmission electron microscopy (HRTEM) were performed using JEOL 3010, 300 kV instrument at an accelerating voltage of 200 kV. Lower accelerating voltage was used to reduce beam-induced damage. Energy dispersive spectra (EDS) were collected using an Oxford Semistem system equipped with the TEM. Samples were dropcasted onto carbon-coated copper grids, 300-mesh, (spi Supplies, 3530C-MB) and dried under ambient condition before examining in TEM.

Theoretical Methods.

Theoretical studies on the electronic and geometric structure of the silver clusters were performed using first principles methods with the Amsterdam Density functional (ADF) code.[39] A generalized gradient approximation (GGA) functional proposed by Perdew, Burke, and Ernzerhof (PBE) was used to incorporate the exchange and correlation effects.[40] Slater-type orbitals (STO) located at the atomic sites we used to express the atomic wave function, and the cluster wave functions were formed via a linear combination of these atomic orbitals. The studies used a TZ2P basis set and a large frozen electron core.[41] The total energies and the forces at the atomic sites we computed and a quasi-Newton method was used to optimize the structures without any symmetry restriction. The energy of the clusters with different spin multiplicities were also calculated to identify the lowest energy structure. Scalar-relativistic effects were included via zero-order regular approximation (ZORA).[42] Time-Dependent Density Functional

Theory, TDDFT, was used to confirm the accuracy of the HOMO-LUMO gaps.

RESULTS AND DISCUSSION

In a typical experiment, the monolayer protected cluster $[Ag_{18}H_{16}(TPP)_{10}]^{2+}$ was prepared as reported previously with some modifications in the synthetic procedure (details are presented in the experimental section).[28] All the characteristic features in the UV-vis spectrum along with the isotopically resolved peak of the molecular ion, $[Ag_{18}H_{16}(TPP)_{10}]^{2+}$ in the electrospray ionization high resolution mass spectrum (ESI HRMS) confirm the identity and purity of the cluster (details are in Supporting Information). The cluster solution is green in color and it shows two peaks in absorption spectroscopy at 545 and 614 nm with a shoulder at 444 nm (Fig. S2(A)). The mass spectrum shows a sharp peak at m/z 2290 in the m/z 1100-5000 window. Expansion of the high resolution mass spectrum shows the isotopic separation of m/z 0.5 due to the 2+ charge state of the parent cluster $[Ag_{18}H_{16}(TPP)_{10}]^{2+}$, matching exactly with the calculated one shown in the corresponding inset (Fig. S2(B) and (C)). The composition of the cluster was further established using G2Si by changing the $NaBH_4$ used for the synthesis to $NaBD_4$, where hydride ions are replaced by deuteride ions forming $[Ag_{18}D_{16}(TPP)_{10}]^{2+}$ (Fig. S3). Due to this replacement, there was a shift in the peak position ($\Delta m/z = 8$, where Δm is 16 and z is +2). Electrosprayed cluster ions were passed through a heating tube to create NCs, which were analyzed by nano-ESI mode of the LTQ mass spectrometer.

  As the G2Si mass spectrometer could not be modified to fit the new ion source needed to prepared outside the mass spectrometer by electrospraying the monolayer protected cluster, conduct these experiments, we have used our LTQ mass spectrometer to detect NCs. A schematic of the set-up is shown in Fig. 1. The heating tube was made of copper (outer diameter 1/8″ and inner diameter 0.066″) with a total length of 50 cm. This copper tube was wrapped with
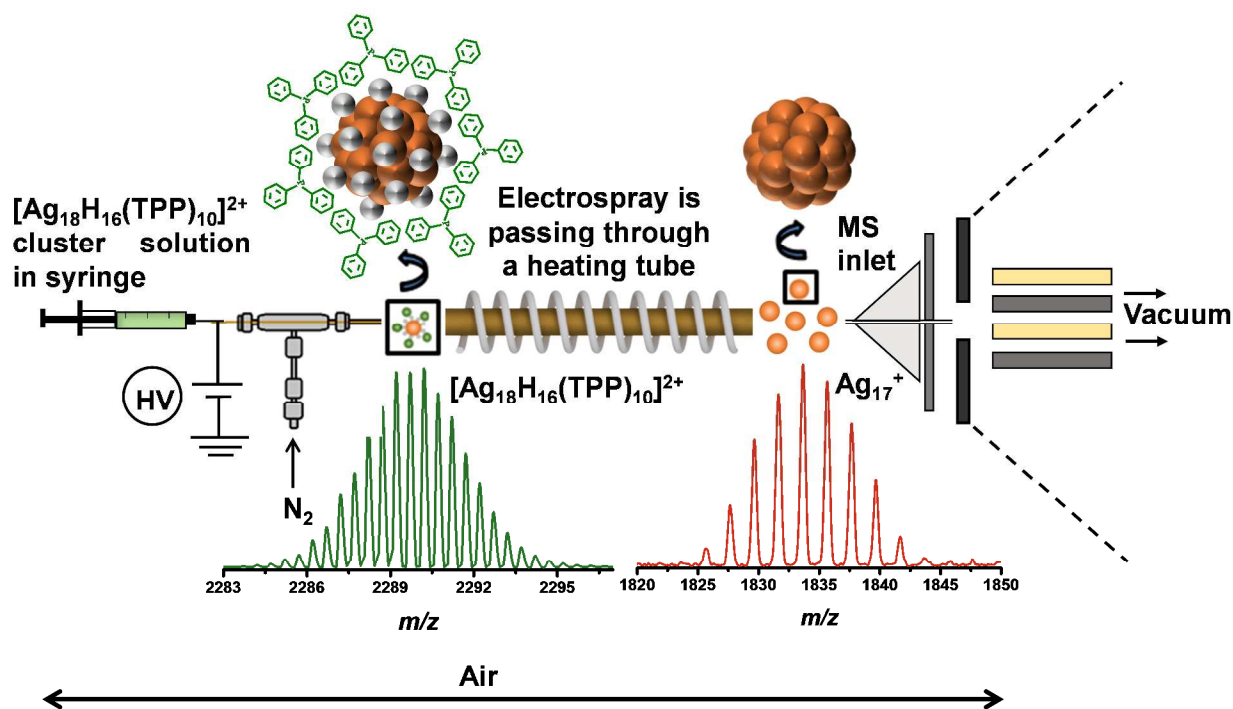
Fig. 1 Schematic representation of experimental set-up where the naked cluster, Ag_{17}^{+} was $[Ag_{18}H_{16}(TPP)_{10}]^{2+}$ through a heated tube and the products were detected by a mass spectrometer. Schematic structures and experimental mass spectra of the corresponding cluster ions are shown in the inset showing that the parent ion is a dication (by using G2Si) and the product is a monocation (by using LTQ). Isotopic separations are therefore m/z 0.5 and 2, respectively.

a heating coil connected to a variable resistance transformer. The exit of the ESI source was inside the heating tube so that maximum ion signal could be obtained. The distance between the heating tube and the inlet of the LTQ mass spectrometer was approximately 5 mm and could be varied. Electrospray of the cluster solution was made at a voltage of +3 kV with N_2 as the nebulizing gas (25 psi pressure). This voltage is important to get a stable ion signal in the mass spectrometer. The temperature of the heating tube was controlled to get the desired species. The ions exiting the heating tube were analyzed by the LTQ mass spectrometer in positive mode under the following conditions to obtain optimized peak intensities: capillary temperature,

250℃; CV, +45 V; TV, +100 V and flow rate, 3 µL/min. Lower than these values of instrumental parameters, the peak intensity was less due to inefficient ionization. With increasing the values of spray voltage (+ 3 kV) and flow rate (3 µL/min), there was no change in peak intensity keeping all other factors the same. Typical injection time was 100 ms and 5 micro scans were averaged to get a good spectrum in all the experiments. To perform the ion/molecule reaction exclusively with O_2 gas, the ions were passed through a Swagelok coupling with different flow rates of O_2 gas. Here, electrospray plays a very important role in the success of the experiment. Without electrospray, we were not able to make these NCs in the gas phase and also study their gas phase reactions.

Continuous monitoring of the mass spectra under various temperatures of the heating tube shows systematic loss of ligands and formation of Ag NCs as shown in Fig. 2. Each ion exhibited isotopically resolved mass spectrum which matched perfectly with its corresponding calculated pattern (Fig. S4). Here the isotopic distribution is mainly due to silver and not due to hydrogen. This is because, ^{107}Ag and ^{109}Ag isotopes of silver are present in almost similar natural abundances (^{107}Ag, 51.839% and ^{109}Ag, 48.161%) but in the case of hydrogen, ^1H has a very high natural abundance (99.98%) in comparison to ^2H and ^3H. The parent cluster $[Ag_{18}H_{16}(TPP)_{10}]^{2+}$ lost the phosphine instantaneously and formed the clusters, $Ag_{17}H_{14}^+$ and $Ag_{18}H_{13}^+$, with peaks centered at m/z 1847 and 1955, respectively. During this conversion process, the charge state of the cluster ion changes from 2+ to 1+ which is confirmed by the isotopic separation of m/z 2 in the resulting cluster ion. Then gradual loss of hydrogen was observed in the mass spectra keeping the charge state constant at 1+ and finally the species Ag_{17}^+ and $Ag_{18}H^+$ were the end products seen, centered at m/z 1833 and 1943, respectively. The ion observed and their charge states can be largely understood from their closed electronic shells.

$Ag_{18}H^+$ (45%) and Ag_{17}^+ (100%) were the only ions in the mass spectrum in the 1100-2000 m/z window. Compared to our previous work where only Ag_{17}^+ was formed by in-source fragmentation of the parent cluster, here both Ag_{17}^+ and $Ag_{18}H^+$ appeared as a result of the thermal ligand desorption from the parent cluster, outside the mass spectrometer. Full range (150-2000 m/z) ESI mass spectrum of this conversion process is shown in Fig. S5 where during
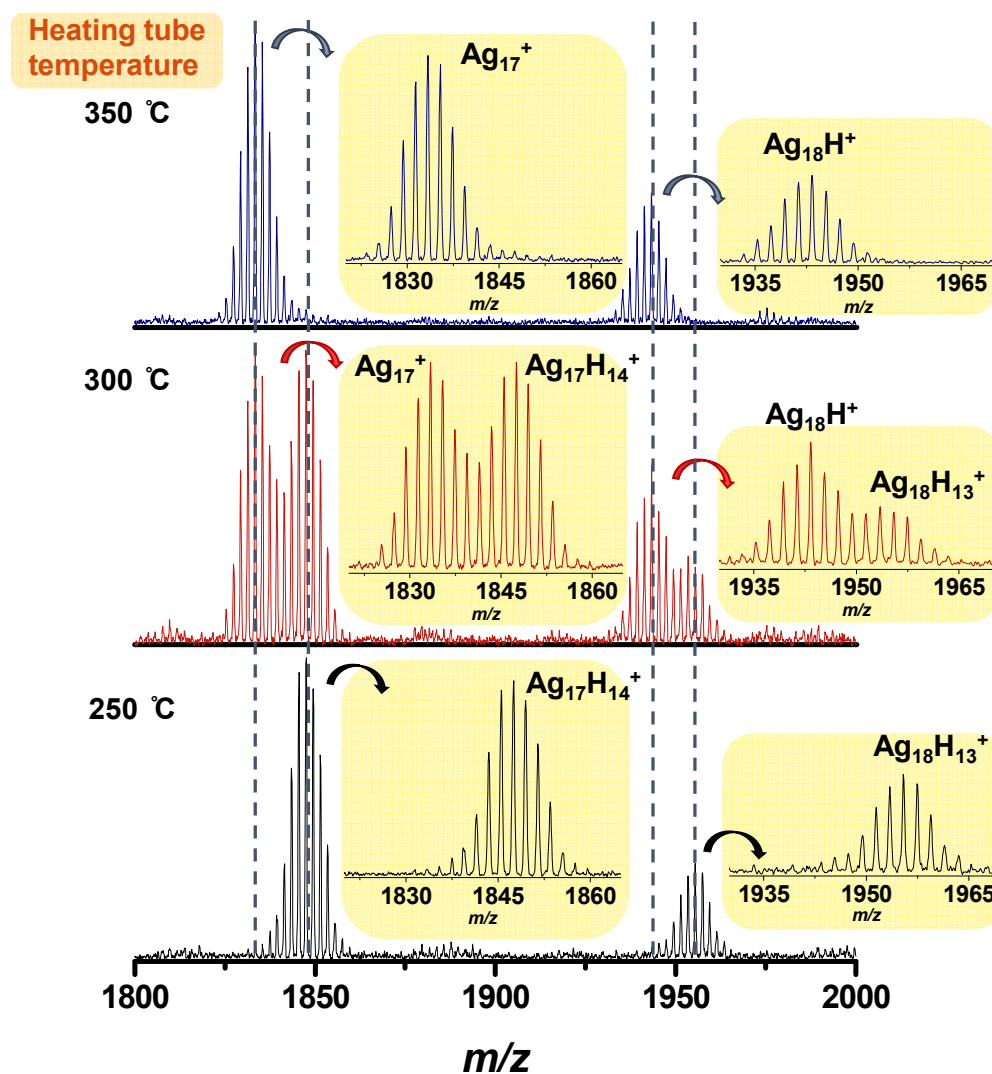
Fig. 2 ESI mass spectrum of $[Ag_{18}H_{16}(TPP)_{10}]^{2+}$ cluster (using LTQ) with varying the temperature of the heating tube. At 250 ℃, $Ag_{17}H_{14}^+$ and $Ag_{18}H_{13}^+$ were detected. At 300℃, Ag_{17}^+ and $Ag_{18}H^+$ were seen along with their hydride clusters and at 350℃ only Ag_{17}^+ and $Ag_{18}H^+$ were seen. Isotopic distributions of these ions are shown in the inset.

heating, oxidation peaks of $[Ag(TPP)]^+$, $[Ag(TPP)_2]^+$ and TPP^+ appear at lower mass region. By this method, we could get both of these products (Ag_{17}^+ and $Ag_{18}H^+$) prepared outside the mass spectrometer, whereas to get selectively any one of these products in 100% relative abundance, we had to do mass selection. However, the ratio of $Ag_{18}H^+$ to Ag_{17}^+ could be changed depending on the transfer medium and the distance between the heating tube and the mass spectrometer inlet. Systematic loss of hydrogen occurs in the form of H_2, as revealed by tandem mass spectrometric studies. The formation of $Ag_{18}H^+$ and Ag_{17}^+ from the precursors, $Ag_{18}H_{13}^+$ and $Ag_{17}H_{14}^+$ proceed through the loss of 6 and 7 dihydrogen species, respectively as shown by independent studies.[29] The conversion process was also studied starting with $[Ag_{18}D_{16}(TPP)_{10}]^{2+}$ instead of $[Ag_{18}H_{16}(TPP)_{10}]^{2+}$. The ESI mass spectrum shows the formation of $Ag_{17}D_{14}^+$ centered at m/z 1861, shifted by 14 mass units from $Ag_{17}H_{14}^+$ ($\Delta m/z = 14$, where Δm is 14 and z is +1). The formation of Ag_{17}^+ via $Ag_{17}D_{14}^+$ confirms the reaction path (Fig. S6). In the mass spectrum of $Ag_{17}D_{14}^+$, 100% exchange of hydrogen with deuterium was not there due to the presence of non-deutereted solvents in the synthesis procedure, which results in additional peaks of lower intensity.

To better understand the formation mechanism of clusters and the fragility of ions, experiments were performed at two sets of CV and TV (a and b) by keeping all other instrumental parameters the same. These conditions are labeled as 1, 2 and 3 in Table 1 and the data are shown in Fig. S7. In one set, the CV and TV were typical instrument parameters, used for all other experiments and were set as 45 V and 100 V, respectively (a). In another set, the CV and TV were set as 140 V and 240 V, respectively (b).

Table 1: Experiments at different instrumental conditions

Expt	Heating tube temp (℃)	CV (V)	TV (V)	Results in between 1100-2000 m/z window
1.a	Room temp	45	100	No silver cluster were detected
1.b	Room temp	140	240	$Ag_{17}H_{14}^{+}$ alone
2.a	250	45	100	$Ag_{17}H_{14}^{+}$ and $Ag_{18}H_{13}^{+}$
2.b	250	140	240	Ag_{17}^{+} along with Ag_{16}^{+} and Ag_{15}^{+}
3.a	350	45	100	Ag_{17}^{+} and $Ag_{18}H^{+}$
3.b	350	140	240	Ag_{17}^{+} and $Ag_{18}H^{+}$ were fragmented partially and appeared along with smaller core size naked silver clusters

These observations make us conclude that when ions were transferred from atmosphere to vacuum, in-source fragmentation occurred at higher CV and TV (expt b), but not at our typical mass spectrometer parameters where CV and TV were set to 45 V and 100 V (expt a). Full range mass spectra as a function of temperature at CV and TV up to 140 V and 240 V, respectively are shown in Fig. S8.

Ion chronograms and MS^2 spectra of selected ions are shown in Fig. S9 and Fig. S10, respectively. The MS^2 spectra of $Ag_{17}H_{14}^{+}$ and $Ag_{18}H^{+}$ gave back the nearest stable NC, Ag_{17}^{+} as a result of hydride and AgH loss, respectively. Similar kind of AgH loss from Ag_nH^{+} (where, n = 2, 4 and 6) was reported before.[43] Whereas the NC Ag_{17}^{+} itself, gave smaller size NCs, Ag_{16}^{+} and Ag_{15}^{+}. It is noteworthy that MS^3 of $Ag_{17}H_{14}^{+}$ and $Ag_{18}H^{+}$ also gave the smaller NCs of silver. The occurrence of $Ag_{18}H^{+}$ instead of Ag_{18}^{+} in the product ions is due to the greater stability of even-numbered electrons in silver clusters as both Ag and H are one electron systems.[44] The same experiment with thiolate protected clusters (Fig. S11) did not create any NCs due to the strong Ag-S bond compared to the weak Ag-P and Ag-H bonds.
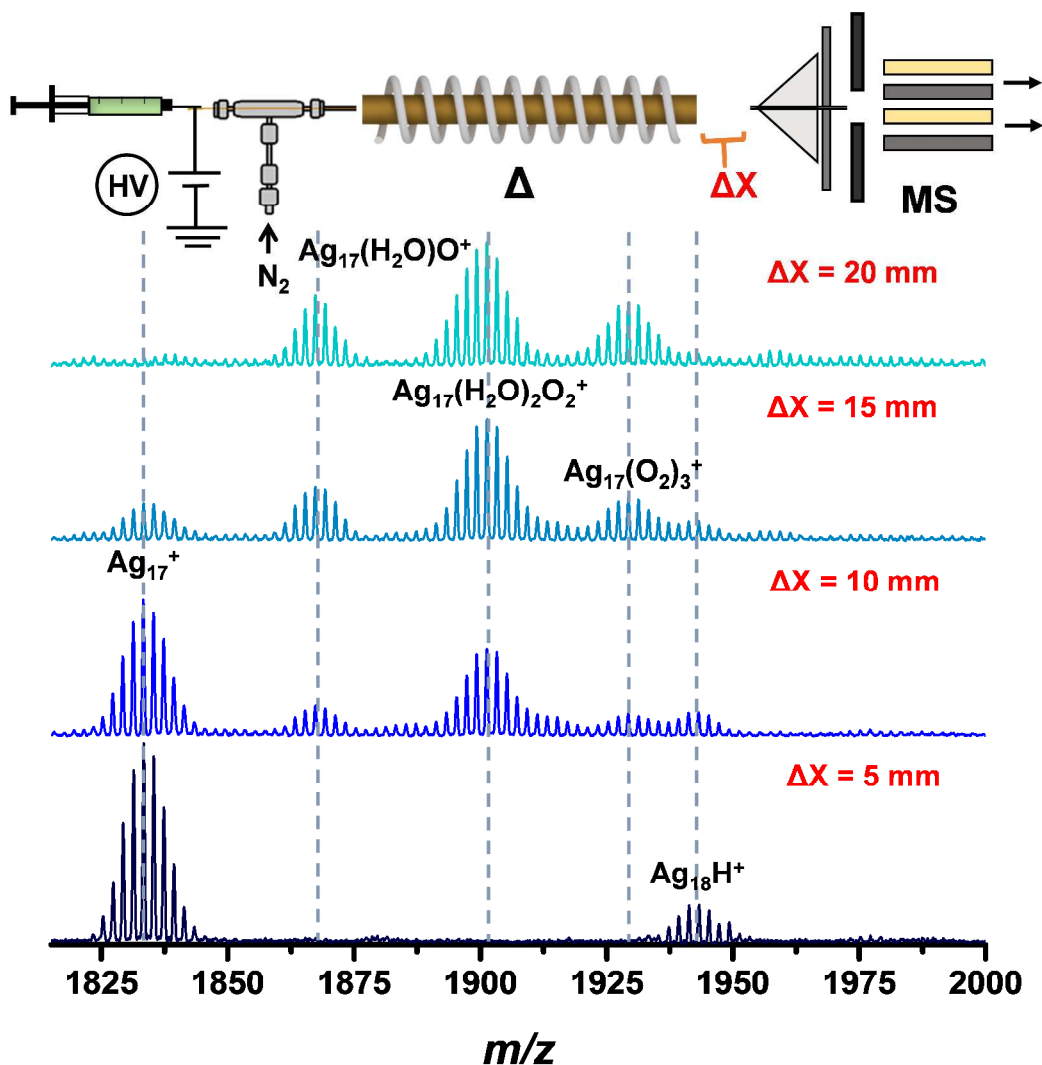
Fig. 3 ESI mass spectrum of Ag_{17}^+ upon varying the distance (ΔX) between the heating tube and the MS inlet (by a moving stage in the xy plane). The peaks observed are a combination of $(H_2O)_m$ and $(O)_n$ additions on the naked cluster, which arise due to air.

  NCs are expected to be highly reactive; however, we find that they can be transported through air, in presence of the nebulizing N_2 gas, without much loss in intensity at a separation of 5 mm between the NC source and the mass spectrometer. This is significant as the distance is 8.4×10^4 times the mean free path of N_2 at standard temperature and pressure (STP). The distance was kept at 5 mm due to the divergence of the ions exiting the heating tube limiting the number of ions collected by the mass spectrometer. The transfer length can be increased further by using a

transfer tube, which confines the ions. Increasing the pressure of the nebulizing gas reduces the transmission loss which also helps in increasing the transfer length and we could increase the length this way to 10 cm.

Experiments were done by varying the distance between the heating tube and the MS inlet to study the reactions of Ag_{17}^+ with atmospheric constituents, at a nebulizer gas pressure of 25 psi (Fig. 3). The intensity of Ag_{17}^+ decreased with the distance due to the addition products of oxygen and water present in the ambient environment. There was mixed oxygen and water addition peaks of Ag_{17}^+ along with oxygen alone species. It was observed that the attachment of water happened only when there was prior oxygen attachment. It is known that water reacts only with pre-oxidized silver clusters of Ag_3^+, Ag_5^+, Ag_7^+, and Ag_9^+, formed by thermal decomposition of silver salts.[32] For $Ag_{18}H^+$, however, no ligation was observed which can be due to its high HOMO-LUMO gap. We also noticed that upon increasing the distance between the ESI source and the heating tube, as ambient air flowed through the heating tube, $Ag_{17}H_{14}^+$ appeared back again. This result is attributed to the lower temperature within the heating tube, favorable for the formation of $Ag_{17}H_{14}^+$ from the parent cluster, $[Ag_{18}H_{16}(TPP)_{10}]^{2+}$ (Fig. S12).

Oxygen was crossed with the flowing mixture of Ag_{17}^+ and $Ag_{18}H^+$ and products as well as unreacted cluster ions were detected with the LTQ at different flow rates of oxygen, as shown in Fig. 4. Photograph and schematic diagram of this set-up used for ion/molecule reaction with oxygen is shown in S13. Ag_{17}^+ shows four oxygen adduct peaks (labeled 1 to 4) and $Ag_{18}H^+$ shows three low intensity oxygen adduct peaks (labeled 1 to 3). For each adduct peak, the isotopic separation is m/z 2, which confirms their 1+ charge state. At low temperature, near about 50 K, O_2 adsorbs (molecular adsorption) on cationic silver clusters as demonstrated for
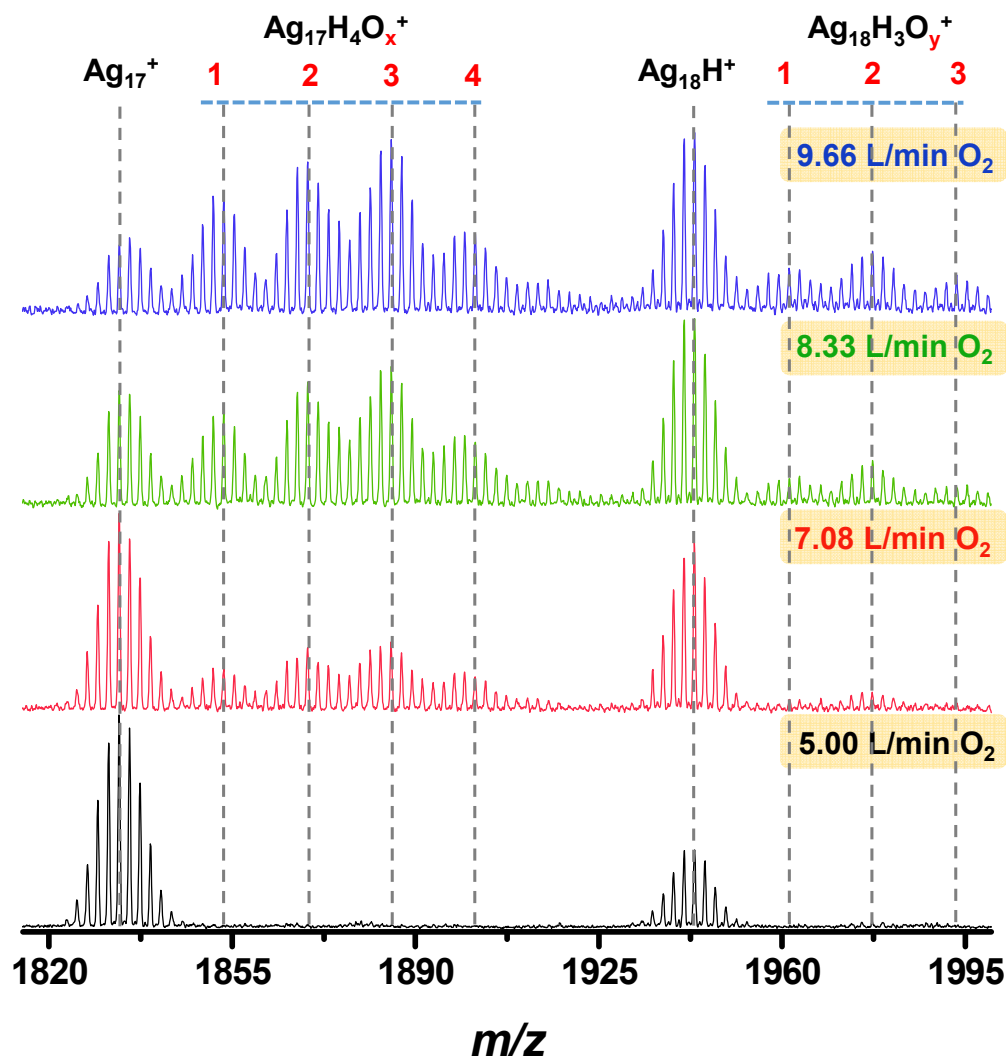
Fig. 4 ESI mass spectrum of Ag_{17}^+ and $Ag_{18}H^+$ ion clusters after reaction with oxygen (O_2) gas at different flow rates.

Ag_2^+.[45] But for hot silver clusters, the absorbed molecular oxygen dissociates to atomic oxygen, resulting in Ag_nO^+ from $Ag_nO_2^+$. Our results suggest dissociative adsorption of oxygen which may be due to the higher temperature used for the preparation of NCs. Several reports studied the mechanism of oxygen adsorption on silver clusters along with their structures, depending on the number of silver atoms and temperature.[46-49] Schmidt et al. reported that due to the positive charge on silver clusters, chemisorption of more than one oxygen molecule, an electron acceptor, is difficult on Ag_n^+ clusters (n < 22) at 77K.[50] But in our experiments, Ag_{17}^+ shows a maximum

adsorption of two oxygen molecules outside the mass spectrometer, though there is an early report of the adsorption of maximum of three oxygen molecules for Ag_2^+ at 120 K.[51] During the oxidation of NCs, in the case of Ag_{17}^+, each oxygen atom addition is followed by four hydrogen atom additions and for the adducts of $Ag_{18}H^+$, there were two hydrogen atom additions. For better understanding of the source of the hydrogens, we have performed experiments in two different ways. In the first case, we have made the $[Ag_{18}H_{16}(TPP)_{10}]^{2+}$ cluster and dissolved it in CD_3OD instead of CH_3OH to understand if there is any role of solvent in the hydrogen attachment. But here we did not observe any different result, as shown in Fig. S14, which made us conclude that hydrogens are not coming from the solvent. In the second case, we have made $[Ag_{18}D_{16}(TPP)_{10}]^{2+}$ by using $NaBD_4$ instead of $NaBH_4$ and dissolved the product in CH_3OH. At a heating tube temperature of 350 ℃, we observed Ag_{17}^+ and $Ag_{18}D^+$ as the NCs and then we have performed the oxygen addition reaction. For $Ag_{17}H_4O_x^+$ and $Ag_{18}H_3O_y^+$, no shifted peaks were seen (Fig. S15A). However, for the $Ag_{18}H_3O_y^+$ peaks, there was some minor contribution from the deuterated species too which appeared as low intense middle peaks, mainly visible for the $Ag_{18}H_3O_2^+$ ion (Fig. S15B). These results made us conclude that water in the ambient environment or within the ion trap is the only source of hydrogen. Comparing the intensities of Ag_{17}^+ and $Ag_{18}H^+$ at different oxygen gas flow rates, we can conclude that $Ag_{18}H^+$ is most abundant at the highest flow rate of oxygen and the relative intensity of Ag_{17}^+ is decreasing faster than $Ag_{18}H^+$ i.e., $Ag_{18}H^+$ is more resistant to oxygen. The plot of relative intensity of Ag_{17}^+ with flow rate of oxygen confirms this (Fig. S16).

We have also performed CID experiments on each of the four oxygen addition peaks of Ag_{17}^+ for a better understanding of their structures (Fig. S17). During collisions with He gas in the trap, collision energy was increased gradually up to the threshold of fragmentation of the precursor

cluster ion. With increasing collision energy, the intensities of the parent cluster ions ($Ag_{17}H_4O^+$, $Ag_{17}H_4O_2^+$, $Ag_{17}H_4O_3^+$ and $Ag_{17}H_4O_4^+$) decayed along with increasing intensity of the fragment ions. For $Ag_{17}H_4O^+$, collisional activation results in the detachment of oxygen and hydrogen atoms and appearance of Ag_{17}^+ as the fragmented ion. $Ag_{17}H_4O_2^+$ fragmented directly to Ag_{17}^+ without giving the $Ag_{17}O^+$ ion, which indicates that it can be molecular adsorption. But in the case of $Ag_{17}H_4O_3^+$ and $Ag_{17}H_4O_4^+$, they go through an intermediate, $Ag_{17}O_2^+$ to Ag_{17}^+. From these results, we see that $Ag_{17}O^+$ and $Ag_{17}O_3^+$ are not formed as intermediates during the fragmentation of $Ag_{17}H_4O_4^+$, which confirms that $Ag_{17}H_4O_4^+$ is formed due to the adsorption of two molecular oxygens. As reported for Ag_2^+, the molecular adsorption peaks were transformed to atomic adsorption peaks by increasing the temperature from 50 K to 130 K.[45] But for Ag_{17}^+, molecular oxygen attachments are seen even at higher temperature. The temperature at which molecular oxygen will dissociate to give atomic oxygen can be varied by the adsorption site or the nano-facet and the presence of defects.[52] Though it is very difficult to interpret, we can assume that our experimental temperature may be lower than the transition temperature needed for adsorbed molecular oxygen on Ag_{17}^+ to dissociate.

During the ion/molecule reactions, from the Figure 3 and 4, it was noted that the ions labelled $Ag_{17}(H_2O)_2O_2^+$ and $Ag_{17}H_4O_4^+$ are having the same elemental composition although their formation methods were different. The first one was made by increasing the distance between the heating tube and the mass spectrometer inlet and the second one was made by the reaction with oxygen gas exclusively. The intensities of $Ag_{17}(H_2O)_2O_2^+$ and $Ag_{17}H_4O_4^+$ were of the order of 10^1 and 10^0, respectively. To get a clearer idea of their structure, we have done CID experiments at the same collision energy, which showed different results for each of them (Fig. S18). From these results, we conclude that though their composition is the same, their structures are

different. In two tables (Table S22, S23) we have summarized the experimental and calculated masses of the assigned clusters observed.

In order to explore the possibility of using the products of electrospray, we have collected the products at heating tube temperatures of 250°C and 350°C, on surfaces held at ambient conditions. The collected products were dispersed in MeOH and $CDCl_3$ to perform ESI mass spectrometry and NMR spectroscopy. Note that MS and NMR studies were conducted after centrifugation to avoid experimental artefacts. No features of hydride protected or NCs were observed in both ESI mass spectra and NMR spectra indicating that the clusters have undergone aggregation. TEM analysis of the products (without centrifugation) confirmed this and the data were compared with that of the $[Ag_{18}H_{16}(TPP)_{10}]^{2+}$ cluster. The parent cluster shows an average particle size 1.68 ± 0.19 nm, whereas the collected electrosprayed products (both at 250°C and 350°C of the heating tube) showed only nanoparticles of variable sizes (Fig. S19). The images suggest that the bare clusters aggregate on the collected surfaces. This leads to poor extraction in solution, unlike organic reaction products.[53] Soft landing on suitable substrates may help their collection without aggregation.[54]

To understand the O_2 resistant reactivity of $Ag_{18}H^+$ we used first-principles theoretical methods and investigated the geometric and electronic structures of Ag_{17}^+ and $Ag_{18}H^+$. As mentioned previously, metal clusters with large HOMO-LUMO gaps tend to be resistant to reactions with O_2, while clusters with unpaired electrons or small HOMO-LUMO gaps are highly reactive with O_2. In the present case, both Ag_{17}^+ and $Ag_{18}H^+$ have an even number of electrons corresponding to 16 and 18 valence electrons. Ag_{17}^+ is found to have an icosahedral core with a 4 atom cap structures decorating the icosahedral core (Fig. 5(A)). The HOMO-
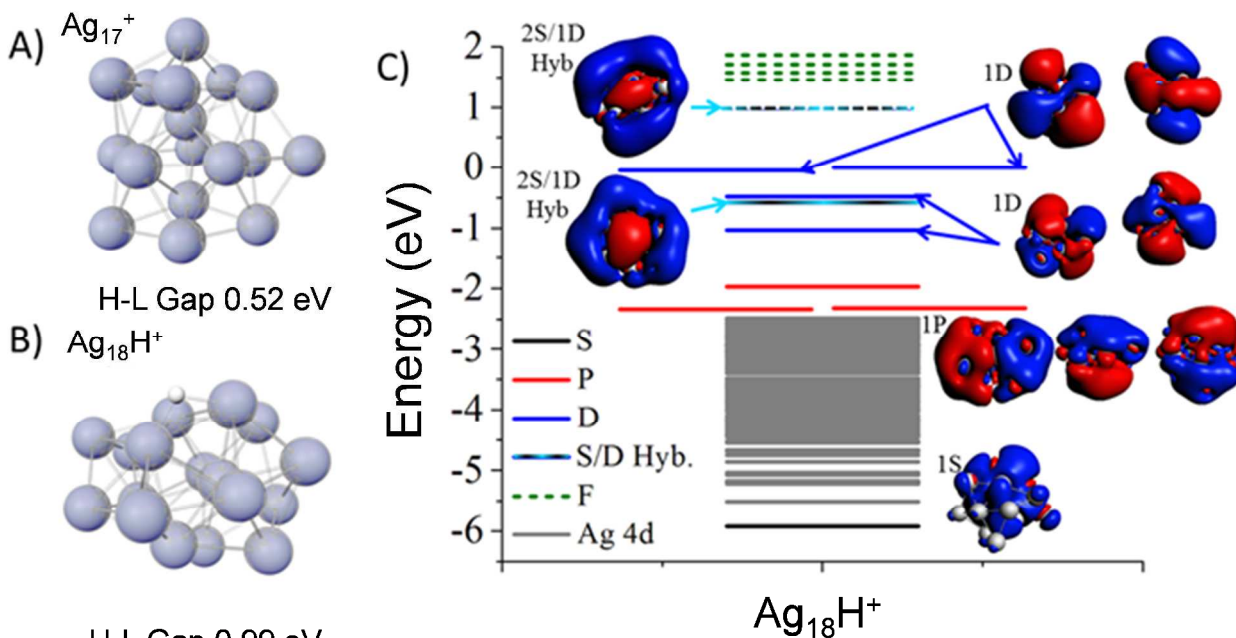
Fig. 5 Structure and HOMO-LUMO gap of (A) Ag_{17}^+ and (B) $Ag_{18}H^+$ clusters. (C) The electronic structure of $Ag_{18}H^+$. The electronic shell structure is $| 1S^2 | 1P^6 | 1D^8\ 2S/1D^2 \| 2S/1D^2 | 1F^{14} |$, with the $1D_z^2$ and 2S orbitals hybridizing.

LUMO gap of Ag_{17}^+ is found to be 0.52 eV, which is a relatively low value, consistent with the cluster being reactive with O_2. Only one isomer within 0.2 eV of the lowest energy structure was found, and it also had a low HOMO-LUMO gap of 0.46 eV. Time-Dependent Density Functional Theory, TD-DFT, was used to confirm the accuracy of the HOMO-LUMO gaps, and we find that the singlet excitation energy for Ag_{17}^+ is 0.47 eV, and the triplet excitation energy is 0.49 eV. Our previous studies on a variety of clusters indicate that metal clusters that are resistant to O_2 reaction when the HOMO-LUMO gaps are typically around or greater than 1 eV (Fig. S20).

$Ag_{18}H^+$ is found to have an oblate structure with HOMO-LUMO gap of 0.99 eV (Fig. 5(B)), large enough to expect the cluster to be resistant to O_2 etching. Alternative structures and their

energetics are given in Fig. S21. TD-DFT finds that the excitation energy and triplet energy for the cluster are 0.94 eV, and triplet excitation energy is 0.96 eV. The H binding energy is 2.26 eV which is approximately equal to the binding energy per atom of H_2, and the ionization potential of $Ag_{18}H^+$ is a relatively low value of 5.25 eV. Each Ag atom provides one valence electron, as does the H atom, so the cluster may be thought of as having 18 valence electrons. The nearest closed electronic shell for silver is expected to be at 20 valence electrons. The relatively large HOMO-LUMO gap may be explained by the oblate structure of the cluster resulting in a splitting of the 1D orbitals giving an electronic structure of $| 1S^2 | 1P^6 | 1D^8\ 1D/2S^2 \| 1D/2S^2 | 1F^{14} |$, as shown in Fig. 5(C). The Ag 4d states (90 states) are shown by the grey region and the double line separates the occupied and unoccupied states. The $1D_z^2$ and the 2S orbitals have the same symmetry, so they hybridize and split due to the oblate structure pushing up in energy the orbitals with more nodes along the compressed axis.[55] The oblate distortion is seen in many of the low energy isomers, with the isomers having HOMO-LUMO gaps between 0.70-1.10 eV. The similar structure of the silver cores results in similar electronic structures in the different isomers, so they may also show enhanced resistance to O_2 reactivity.

CONCLUSIONS

We conclude that naked metal cluster ions can be formed outside the mass spectrometer starting from ligand protected, atomically precise clusters prepared in solution. The reactivity of these NCs to oxygen shows selectivity, which depends on their HOMO-LUMO gaps. It is likely that atmospheric gas phase NCs can be used as reagents and catalysts. They may be deposited on suitable support to create useful materials. Again the oxidized silver clusters can also be used as an oxidizing agent to oxidize CO or NO_2. We have studied various phosphine protected silver clusters ($[Ag_{18}H_{16}(TPP)_{10}]^{2+}$ and $[Ag_{25}H_{22}(DPPE)_8]^{2+}$ (DPPE = 1,2-

bis(diphenylphosphino)ethane)) and thiolate protected silver clusters ($[Ag_{25}(DMBT)_{18}]^{3-}$ (DMBT = 2,4-dimethylbenzenethiol), $[Ag_{44}(FTP)_{30}]^{4-}$ (FTP = 4-fluorothiophenol) and $[Ag_{59}(DCBT)_{32}]^{3-}$ (DCBT = 2,5-dichlorobenzenethiol)), and gold clusters ($[Au_{25}(PET)_{18}]^{-}$ (PET = 2-phenylethanethiol)), available in our laboratory.[6,7,28] From all of these experiments, we conclude that $[Ag_{18}H_{16}(TPP)_{10}]^{2+}$ alone form silver NCs outside the mass spectrometer.

ASSOCIATED CONTENT

Supporting Information. Photograph of the instrumental set-up; characterization of $[Ag_{18}H_{16}(TPP)_{10}]^{2+}$ and $[Ag_{18}D_{16}(TPP)_{10}]^{2+}$ clusters; comparison between the experimental and the calculated spectra; formation of Ag_{17}^{+} from both $Ag_{17}H_{14}^{+}$ and $Ag_{17}D_{14}^{+}$; full range ESI mass spectrum of $[Ag_{18}H_{16}(TPP)_{10}]^{2+}$ cluster during heating and comparison at different capillary and tube lens voltage; full range ESI mass spectrum of $[Ag_{18}H_{16}(TPP)_{10}]^{2+}$ cluster during heating at higher capillary and tube lens voltage; ion chronograms of selected ions; MS^2 for Ag_{17}^{+}, $Ag_{17}H_{14}^{+}$ and $Ag_{18}H^{+}$ ions; thermal dissociation of thiolate protected cluster with same experimental conditions; effect of distance between the heating tube and the ESI source; photograph of the instrumental set-up and diagram used for ion/molecule reactions; comparison of oxygen addition reaction of naked clusters with CD_3OD as solvent and with deuterated analog of $[Ag_{18}H_{16}(TPP)_{10}]^{2+}$; comparison of reactivity between Ag_{17}^{+} and $Ag_{18}H^{+}$ ions with oxygen; MS^2 of $Ag_{17}H_4O^{+}$, $Ag_{17}H_4O_2^{+}$, $Ag_{17}H_4O_3^{+}$ and $Ag_{17}H_4O_4^{+}$ ions; comparison of MS^2 results of $Ag_{17}(H_2O)_2O_2^{+}$ and $Ag_{17}H_4O_4^{+}$ ions; TEM images of $[Ag_{18}H_{16}(TPP)_{10}]^{2+}$ cluster and the electrosprayed products collected; calculated structures of Ag_{15}^{+}, Ag_{17}^{+}, Ag_{18}^{+}, and $Ag_{18}H^{+}$ ions; isomers of $Ag_{18}H^{+}$ and their energies; experimental and calculated masses measured by using the LTQ and G2Si (PDF).

AUTHOR INFORMATION

Corresponding Authors

* Email: pradeep@iitm.ac.in

* Email: snkhanna@vcu.edu

Notes

The authors declare no competing financial interests.

ACKNOWLEDGMENTS

REFERENCES

1. R. L. Whetten, J. T. Khoury, M. M. Alvarez, S. Murthy, I. Vezmar, Z. L. Wang, P. W. Stephens, C. L. Cleveland, W. D. Luedtke and U. Landman, *Adv. Mater.*, 1996, **8**, 428-433.
2. R. Jin, *Nanoscale*, 2015, **7**, 1549-1565.
3. P. Maity, S. Xie, M. Yamauchi and T. Tsukuda, *Nanoscale*, 2012, **4**, 4027-4037.
4. W. Kurashige, Y. Niihori, S. Sharma and Y. Negishi, *J. Phys. Chem. Lett.*, 2014, **5**, 4134-4142.
5. S. Knoppe and T. Bürgi, *Acc. Chem. Res.*, 2014, **47**, 1318-1326.
6. I. Chakraborty and T. Pradeep, *Chem. Rev.*, 2017, **117**, 8208-8271.
7. R. Jin, C. Zeng, M. Zhou and Y. Chen, *Chem. Rev.*, 2016, **116**, 10346-10413.
8. G. Schmid and N. Klein, *Angew. Chem. Int. Ed. Engl.*, 1986, **25**, 922-923.
9. P.-T. Chen, E. C. Tyo, M. Hayashi, M. J. Pellin, O. Safonova, M. Nachtegaal, J. A. van Bokhoven, S. Vajda and P. Zapol, *J. Phys. Chem. C*, 2017, **121**, 6614-6625.
10. S. Lee, C. Fan, T. Wu and S. L. Anderson, *J. Am. Chem. Soc.*, 2004, **126**, 5682-5683.
11. H. Tsunoyama, N. Ichikuni, H. Sakurai and T. Tsukuda, *J. Am. Chem. Soc.*, 2009, **131**, 7086-7093.
12. Z. Wu, G. Hu, D.-e. Jiang, D. R. Mullins, Q.-F. Zhang, L. F. Allard, L.-S. Wang and S. H. Overbury, *Nano Lett.*, 2016, **16**, 6560-6567.
13. I. Diez and R. H. A. Ras, *Nanoscale*, 2011, **3**, 1963-1970.

14. M. Turner, V. B. Golovko, O. P. H. Vaughan, P. Abdulkin, A. Berenguer-Murcia, M. S. Tikhov, B. F. G. Johnson and R. M. Lambert, *Nature*, 2008, **454**, 981.

15. K. P. Kerns, B. C. Guo, H. T. Deng and A. W. Castleman, *J. Chem. Phys.*, 1994, **101**, 8529-8534.

16. L. A. Angel, L. T. Majors, A. C. Dharmaratne and A. Dass, *ACS Nano*, 2010, **4**, 4691-4700.

17. A. Baksi, S. R. Harvey, G. Natarajan, V. H. Wysocki and T. Pradeep, *Chem. Comm.*, 2016, **52**, 3805-3808.

18. Z. Luo, A. W. Castleman and S. N. Khanna, *Chem. Rev.*, 2016, **116**, 14456-14492.

19. T. E. Dermota, Q. Zhong and A. W. Castleman, *Chem. Rev.*, 2004, **104**, 1861-1886.

20. S. J. Riley, *Ber. Bunsenges. phys. Chem.*, 1992, **96**, 1104-1109.

21. D. M. Black, C. M. Crittenden, J. S. Brodbelt and R. L. Whetten, *J. Phys. Chem. Lett.*, 2017, **8**, 1283-1289.

22. M. G. Taylor and G. Mpourmpakis, *Nat. Commun.*, 2017, **8**, 15988.

23. P. Chakraborty, A. Baksi, E. Khatun, A. Nag, A. Ghosh and T. Pradeep, *J. Phys. Chem. C*, 2017, **121**, 10971-10981.

24. R. Jin, S. Zhao, Y. Xing and R. Jin, *CrystEngComm*, 2016, **18**, 3996-4005.

25. M. Krstić, A. Zavras, G. N. Khairallah, P. Dugourd, V. Bonačić-Koutecký and R. A. J. O'Hair, *Int. J. Mass Spectrom.*, 2017, **413**, 97-105.

26. M. Girod, M. Krstić, R. Antoine, L. MacAleese, J. Lemoine, A. Zavras, G. N. Khairallah, V. Bonačić-Koutecký, P. Dugourd and R. A. J. O'Hair, *Chem. Eur. J.*, 2014, **20**, 16626-16633.

27. A. J. Jordan, G. Lalic and J. P. Sadighi, *Chem. Rev.*, 2016, **116**, 8318-8372.

28. M. S. Bootharaju, R. Dey, L. E. Gevers, M. N. Hedhili, J.-M. Basset and O. M. Bakr, *J. Am. Chem. Soc.*, 2016, **138**, 13770-13773.

29. A. Ghosh, M. Bodiuzzaman, A. Nag, M. Jash, A. Baksi and T. Pradeep, *ACS Nano*, 2017, **11**, 11145-11151.

30. H. Chen, L. S. Eberlin and R. G. Cooks, *J. Am. Chem. Soc.*, 2007, **129**, 5880-5886.

31. L. S. Eberlin, Y. Xia, H. Chen and R. G. Cooks, *J. Am. Soc. Mass Spectrom.*, 2008, **19**, 1897-1905.

32. M. Wleklinski, D. Sarkar, A. Hollerbach, T. Pradeep and R. G. Cooks, *Phys. Chem. Chem. Phys.*, 2015, **17**, 18364-18373.

33. B. D. Leskiw, A. W. C. Jr., C. Ashman and S. N. Khanna, *J. Chem. Phys.*, 2001, **114**, 1165-1169.

34. H. Häkkinen, *Adv. Phys.: X*, 2016, **1**, 467-491.

35. S. Klacar, A. Hellman, I. Panas and H. Grönbeck, *J. Phys. Chem. C*, 2010, **114**, 12610-12617.

36. A. W. Castleman and S. N. Khanna, *J. Phys. Chem. C*, 2009, **113**, 2664-2675.

37. A. C. Reber, S. N. Khanna, P. J. Roach, W. H. Woodward and A. W. Castleman, *J. Am. Chem. Soc.*, 2007, **129**, 16098-16101.

38. Z. Luo, G. U. Gamboa, J. C. Smith, A. C. Reber, J. U. Reveles, S. N. Khanna and A. W. Castleman, *J. Am. Chem. Soc.*, 2012, **134**, 18973-18978.

39. G. te Velde, F. M. Bickelhaupt, E. J. Baerends, C. Fonseca Guerra, S. J. A. van Gisbergen, J. G. Snijders and T. Ziegler, *J. Comput. Chem.*, 2001, **22**, 931-967.

40. J. P. Perdew, K. Burke and M. Ernzerhof, *Phys. Rev. Lett.*, 1996, **77**, 3865-3868.

41. E. Van Lenthe and E. J. Baerends, *J. Comput. Chem.*, 2003, **24**, 1142-1156.

42. E. van Lenthe, E. J. Baerends and J. G. Snijders, *J. Chem. Phys.*, 1994, **101**, 9783-9792.

43. G. N. Khairallah and R. A. J. O'Hair, *Dalton Trans.*, 2005, DOI: 10.1039/B505645B, 2702-2712.

44. R. Fournier, *J. Chem. Phys.*, 2001, **115**, 2165-2177.

45. L. D. Socaciu, J. Hagen, U. Heiz, T. M. Bernhardt, T. Leisner and L. Wöste, *Chem. Phys. Lett.*, 2001, **340**, 282-288.

46. M. Schmidt, A. Masson and C. Bréchignac, *Phys. Rev. Lett.*, 2003, **91**, 243401.

47. M. Schmidt, P. Cahuzac, C. Bréchignac and H.-P. Cheng, *J. Chem. Phys.*, 2003, **118**, 10956-10962.

48. Y.-N. Wu, M. Schmidt, J. Leygnier, H.-P. Cheng, A. Masson and C. Bréchignac, *J. Chem. Phys.*, 2012, **136**, 024314.

49. T. M. Bernhardt, *Int. J. Mass Spectrom.*, 2005, **243**, 1-29.

50. M. Schmidt, A. Masson, H.-P. Cheng and C. Bréchignac, *ChemPhysChem*, 2015, **16**, 855-865.

51. M. J. Manard, P. R. Kemper and M. T. Bowers, *Int. J. Mass Spectrom.*, 2003, **228**, 865-877.
52. L. Vattuone, L. Savio and M. Rocca, *Phys. Rev. Lett.*, 2003, **90**, 228302.
53. P. Liu, R. G. Cooks and H. Chen, *Angew. Chem. Int. Ed.*, 2015, **54**, 1547-1550.
54. J. Laskin, G. E. Johnson, J. Warneke and V. Prabhakaran, *Angew. Chem. Int. Ed. Engl.*, 2018.
55. A. C. Reber and S. N. Khanna, *Acc. Chem. Res.*, 2017, **50**, 255-263.

TOC GRAPHICS